Screening for Diabetic Retinopathy Using Computer Vision and Physiological Markers

The definitive version of this paper can be found at:

Hann, C.E., Hewett, D., Revie, J.A., Chase, J.G. and Shaw, G.M. (2009) *Screening for Diabetic Retinopathy Using Computer Vision and Physiological Markers*. J Diabetes Sci Technol 2009;3(4):819-834
http://www.journalofdst.org/July2009/Articles/VOL-3-4-ORG4-HANN.pdf

Short Title: **Diabetic Retinopathy Screening via Computer Vision**

Keywords: diabetes, diabetic retinopathy, computer vision, image processing, digital images, fundus images

Funding, Acknowledgements, Disclosures:

⇒ This study was not specifically funded
⇒ The authors declare no conflicts of interest with respect to this work (none)

Christopher E. Hann[1], PhD, BSc
James A. Revie[2], BE(Hons)
Darren Hewett[2], BE(Hons)
J. Geoffrey Chase[3], BS, MS, PhD
Geoffrey M. Shaw[4], MBChB, FANCZA, FJFICM

[1] Sir Charles Hercus Health Research Fellow, University of Canterbury, Centre for Bio-Engineering, Department of Mechanical Engineering, Private Bag 4800, Christchurch, New Zealand
Email: chris.hann@canterbury.ac.nz

[2] Research Assistant, University of Canterbury, Centre for Bio-Engineering, Department of Mechanical Engineering, Private Bag 4800, Christchurch, New Zealand

[3] Prof., University of Canterbury, Centre for Bio-Engineering, Department of Mechanical Engineering, Private Bag 4800, Christchurch, New Zealand

Honorary Senior Lecturer, Christchurch School of Medicine and Health Sciences, University of Otago, Christchurch, New Zealand.
Email: geoff.chase@canterbury.ac.nz

[4] Clinical Sr. Lecturer University of Otago School of Medicine, Christchurch, New Zealand
Senior Consultant, Department of Intensive Care, Christchurch Hospital, New Zealand

ABSTRACT

Background: Hyperglycemia and diabetes result in vascular complications, most notably diabetic retinopathy (DR). The prevalence of DR is growing and it is a leading cause of blindness and/or visual impairment in developed countries. Current methods of detecting, screening and monitoring DR are based on subjective human evaluation, which is also slow and time consuming. As a result, the initiation and progress monitoring of DR is clinically hard.

Methods: Computer vision methods are developed to isolate and detect two of the most common DR dysfunctions, dot hemorrhages (DH) and exudates. The algorithms use specific colour channels and segmentation methods to separate these DR manifestations from physiological features in digital fundus images. The algorithms are tested on the first 100 images from a published database. Diagnostic outcome and the resulting positive and negative prediction values (PPV and NPV) are reported. The first 50 images are marked with specialist determined ground truth for each individual exudate and/or DH, which are also compared to algorithm identification.

Results: Exudate identification had 96.7% sensitivity and 94.9% specificity for diagnosis (PPV = 97%, NPV = 95%). DH identification had 98.7% sensitivity and 100% specificity (PPV = 100%, NPV = 96%). Greater than 95% of ground truth identified exudates and DHs were found by the algorithm in the marked first 50 images, with less than 0.5% false positives.

Conclusions: A direct computer vision approach enabled high quality identification of exudates and DHs in an independent dataset of fundus images. The methods are readily generalisable to other clinical manifestations of DR. The results justify a blinded clinical trial of the system to prove its capability to detect, diagnose and, over the long term, monitor the state of DR in diabetic individuals.

1. Introduction

Diabetic Retinopathy (DR) is one of the main causes of blindness and visual impairment in developed countries [1-2]. In the United States the prevalence rates of retinopathy and vision threatening retinopathy are estimated to be 40.3% and 8.2% respectively for diabetic adults 40 years or older [3]. Within the next 15 to 30 years the number of people with diabetes is expected to double due to factors such as obesity, an aging population and inactive lifestyles [4]. Studies have shown that early detection combined with appropriate treatment and management can prevent the loss of vision in up to 95% of cases [2, 5-7]. DR is the manifestation of systemic disease which affects up to 80% of all patients who have had diabetes for 10 years or more [8]. The high prevalence of diabetes therefore makes mass screening an expensive and time consuming process.

It has been shown that an automated system could greatly reduce the workload by filtering out 50% of the screening population [9]. Recently, a large retrospective analysis of 10,000 consecutive patient visits was performed [10], but it was concluded that automated detection of DR using published algorithms cannot yet be recommended for clinical practice. In addition, it was also concluded [10], that if the algorithms can be improved, such a system may lead to improved prevention of blindness and vision loss in patients with diabetes.

DR results from leakage of small vessels in the retina correlated to a prolonged period of hyperglycaemia. In the early stages of the disease known as nonproliferative retinopathy, there may be hemorrhages due to bleeding of the capillaries or exudates resulting from protein deposits in the retina. There is usually no vision loss unless there is a build up of fluid in the centre of the eye. As the disease progresses, new abnormal vessels grow in the retina, known as

neovascularization. These vessels frequently leak into the vitreous. This stage of the disease is called proliferative retinopathy and may cause severe visual problems. The goal of the screening system is to detect the nonproliferative stage of DR so the disease can be appropriately managed to decrease the chances of vision impairment.

The use of seven-field stereo fundus photography read by a trained reader to diagnose DR is the current, non-invasive gold standard. DR grading using the fundus images is significantly more sensitive that standard opthalmoscopy, which can miss approximately 50% of subjects with only microaneurysms, resulting in under reporting of DR prevalence rates by approximately 10% [11,12]. Recent research has demonstrated combining fundus photography and computer algorithms to automatically grade DR (e.g. [10]). These algorithms search for bad lesions in the fundus images, which define the severity of DR. The lesions are categorised into microaneurysms, hemorrhages and exudates based on their location, morphology and colour. However, most rely on training sets that are human marked or graded, thus introducing subjective evaluation.

Thus, a method developed by Sanchez et al to detect hard exudates produced a sensitivity of 88% with an average of 4.83 false positives per image [13]. Walter et al. developed a method to detect microaneurysms and obtained a sensitivity of 88.5% with an average of 2.13 false positives per image [14]. For the problem of just detecting DR, the method of [15] correctly identified 90.1% of patients with retinopathy and 81.3% of patients without retinopathy. Therefore in [15] there are 18.7% false positives, which is quite large and is a typical problem in most methods. As noted, the most common current approaches to automating DR screening are statistical classifying methods [9, 13-15], and/or neural networks and similar methods [16,17].

This paper takes an alternative more analytical approach by focusing on direct identification using accurate geometric models at the pre-processing stage. Two independent algorithms are developed to detect exudates and dot hemorrhages (DHs). Information from the colour, morphology and intensity gradients of the fundus photograph provide the means to detect the number of exudates and DHs, and thus to determine the presence of DR. It uses additional standard computer vision algorithms to identify and eliminate false positives, without reducing true positive results. Overall, this paper thus focuses on the problem of accurately detecting DR, rather than just grading images, which is a salient difference from most prior work. In addition, it focuses on identifying lesions or diseases independently, rather than all at once, even though only the one image is used. Finally, it is thus based on directly identifying physiologically observed states and uses that information directly, which some other approaches ignore in whole or part.

2.0 Methodology

Two separate algorithms are written for automatically detecting exudates and dot haemorrhages. The algorithms were developed based on fundus images from the Diaret dbO_v_1_1 database [19, 20]. The images are were captured using a 50 degree field-of-view and resolution of 1.5 M pixels. The imaging noise, optical aberrations, and accuracy of the photometric information are unknown for the photographs. Note that the images from the database do not correspond to any typical population, but were dedicatedly selected, so that the sample is biased [20]. The types of DR present in the images were dot haemorrhages, exudates, microaneurysms and neovascularisation. A non-DR related lesion is drusen. Drusen are bright lesions associated especially with age-related macular degeneration, which can have a similar appearance to exudates [21]. However, no drusen was reported in the ground truths of the data base, therefore

it was not possible to develop an algorithm to differentiate between drusen and exudates. Future work will address this issue. The two methods used to test the images for dot hemorrhages and exudates, are outlined in separate sections with a summary at the end.

2.1 Exudate Detection

Exudates are common abnormalities in the retina of diabetic patients. Exudates are bright lipid leaked from a blood vessel. The leaked fluid tends to stay close to the lesion giving a generally well-defined edge suitable for computer analysis, e.g. [18].

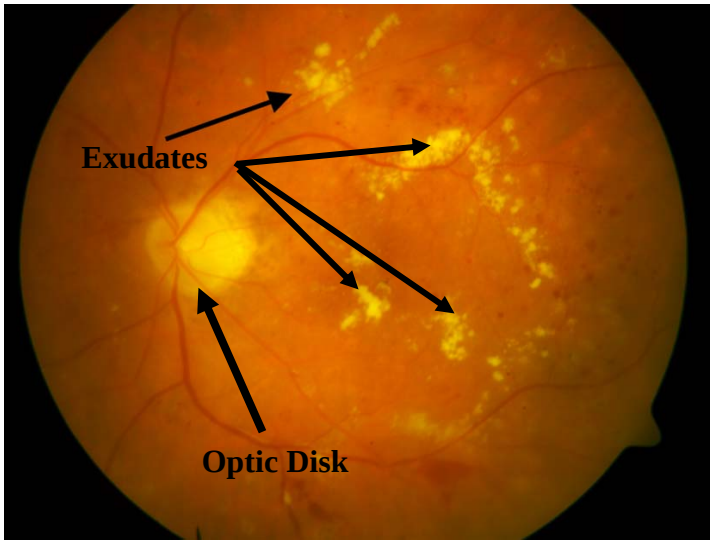

Figure 1: Exudates and optic disk.

Figure 1 gives an example of exudates on a fundus image, which show up as small, light yellow regions. In practice the "light" part of the image, shows up as a high number in terms of the intensities that represent the image. Intensities are always numbers between 0 and 255 with 0 being the darkest pixel and 255 the lightest. There are three channels, red, green and blue which each have a matrix of numbers between 0 and 255. The matrix covers the whole image and it's

size depends on the resolution of the camera. Note that since the intensities are a unitless representation of how "light" a pixel is, no units are given in all the figures in this paper.

The optic disc, which can be seen in Figure 1, is also a light yellow region. Therefore, before searching for exudates based on their yellow colour, an algorithm is developed for automatic detection of the optic disc to eliminate this physiologically valid, yet similar appearing structure. The yellow colour corresponds to a high intensity on the green channel and typically the optic disc contains the majority of the highest green intensities on a given image. Therefore an initial approximation to the optic disc is obtained by sorting the green intensities from the lowest to the highest, and choosing all pixels in the top 0.5% of intensities. This method may also capture some other bright yellow regions like exudates but the majority will lie on the optic disc. Figure 2(a) gives the results after zooming in on the region which contains all the detected pixels.

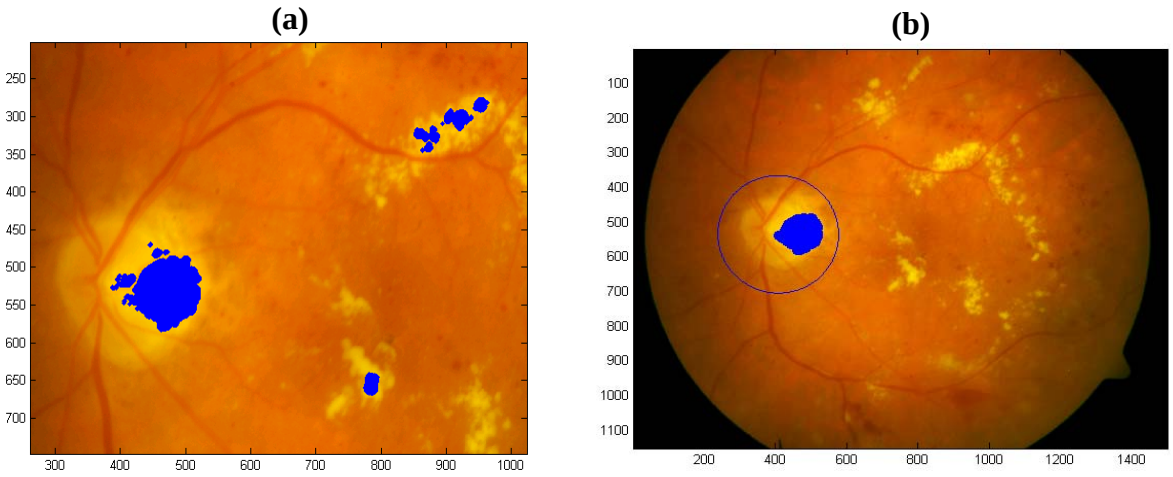

Figure 2: (a) The result of choosing the top 0.5% of the green intensities (b) Locating the optic disc based on the largest connected region. The region is bounded by a cricle

Notice in Figure 2(a), that the largest connected region (LCR) lies on one half of the optic disc. In standardized macula photos the LCR is always on the side of the largest distance between the centre of the optic disk and the vertical edge of the image. For the example in Figures 1 and 2(a), the largest distance corresponds to the right half of the disc. Therefore the LCR lies to the right of the disk centre. However, in a reasonable number of images the centre of the optic disc lies in the right half of the whole image in Figure1. In this case, the LCR lies to the left of the centre of the optic disc, but is easily accommodated in the algorithm. This property was found to be consistent over all 100 images in the database considered [19, 20], with no exceptions. Note that the algorithm is equally applicable to both left and right eyes.

Hence, a simple and robust way of locating the optic disc is to place a rectangle precisely containing the LCR, and define a circle with the centre at the left edge mid-point and radius the horizontal width of the rectangle. To ensure this computed circle always bounds the optic disc the radius is increased by 50%. Figure 2(b) shows the LCR and the resulting circular bound containing the optic disc.

The next step is to approximately equalize the contrast in the green channel to allow an initial sweep of the image to find potential candidates for exudates. The contrast is equalized by first computing a 50 pixel median filter in the horizontal and vertical directions. The value of 50 pixels refers to the number of pixels on each side of a given pixel over which the median is computed. The minimum of the median in each direction is then subtracted from each pixel intensity in the image. Median filtering is a well known method to remove slow gradients over the image and is sometimes referred to as “shade correction” [21].

Figure 3 gives an example Image 029 from the database, before contrast equalisation is applied. A vertical (blue) line is shown through the pixel position x = 153. Figure 4(a) shows the green intensities plotted along the vertical line in Figure 3.

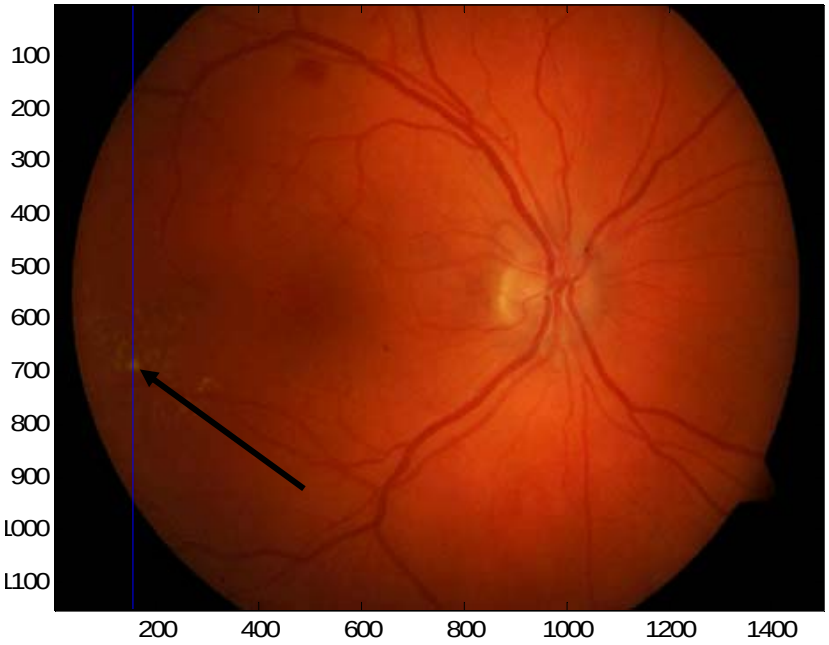

Figure 3: Image 029 from the database with a blue line through x = 153 and an exudate pointed out with an arrow.

In Figure 3 it is clear there is an exudate at (x,y) = (153,684), which is pointed out with the arrow. This point shows up as a sharp peak in Figure 4(a). The result after performing a contrast equalisation is shown in Figure 4(b). Notice that the jumps at the beginning and ending of Figure4 (a) are removed. These jumps correspond to the transition between the light (orange colored) and dark (due to fundus mask) regions of Figure 3. The slight increasing trend from y =

200 to 800 is also removed, but the major peak still remains in Figure 4 (b) to identify the exudate. This approach ensures exudates will stand out more equally in dark or light areas.

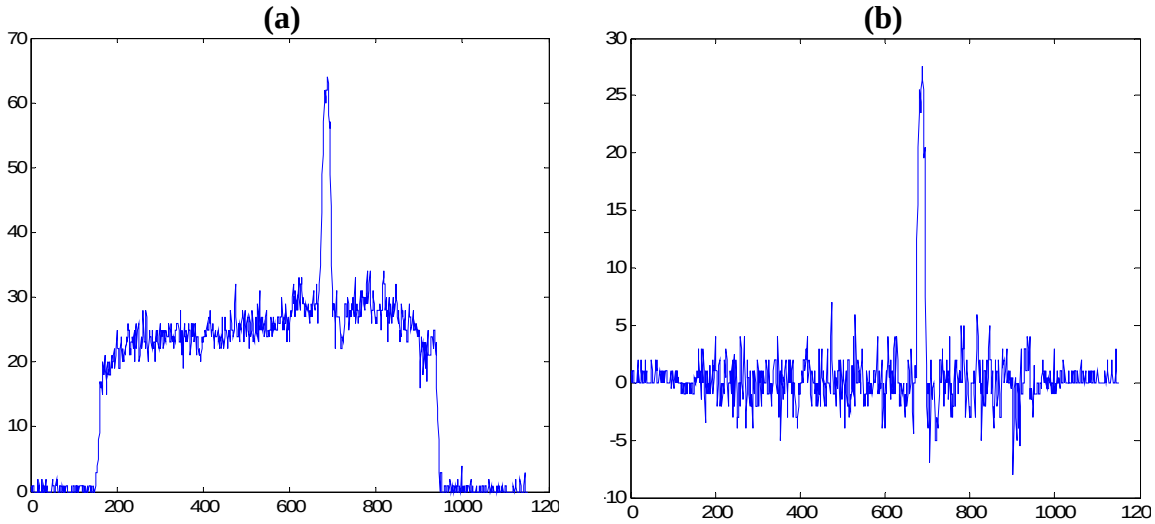

Figure 4: (a) Plotting the green intensity along the line shown in Figure 3. (b) The result of subtracting the 50 pixel median from each intensity

Based on several darker images in the database where exudates had a lower contrast to the background, a threshold of 10 was chosen to guarantee finding an exudate when it exists. The same procedure described above is applied to horizontal lines of constant y value, similar to the vertical line in Figure 3. The union of the selected pixels for potential exudates in both the horizontal and vertical directions are chosen as potential exudate locations. Thus, every pixel is also examined in this approach across both dimensions of the image.

The next part of the method then removes any pixels that are clearly not exudates. For example any pixels that lie inside the optic disc or have very low intensities corresponding to the very dark regions of Figure 3 are removed. If the number of pixels in a connected region is less than a given tolerance, it is considered too small to be an exudate and is likely a small spot in the image that may occur for any number of reasons. Thus, this small region is removed as well.

The algorithm then adds pixels to each of the remaining potential exudate regions that may have been missed by the initial sweep. For example, Figure 5(a) is the result of detected exudates after applying the median filter method resulting Figure 4(b). The method detects the presence of exudates, but several areas that are part of an exudate are not covered. To add more pixels, all the connected regions in Figure 5(a) that have a sufficiently high maximum green intensity and contain pixels with a contrast equalized intensity greater than 30 are added. This test ensures that any extra pixels added are always onto an actual exudate. The threshold of 30 was determined by trial and error and ensures pixels will not be added to exudates in lower contrast and darker regions of the image. However, the main purpose of this method is to better cover the cases where there are very clear exudates, such as those shown in Figure 1. Furthermore, by adding pixels, large, more obvious exudates can be removed to save computational time when more sophisticated methods are used to confirm smaller exudates in the lower contrast regions.

For each chosen connected pixel region, all the red/green intensity ratio are ordered from the lowest to the highest. Two intensities I_{low} and I_{high} are chosen. The first intensity I_{low} corresponds to the intensity such that only 5% of all intensities are smaller than I_{low}. Mathematically, I_{low} denotes the lower 5^{th} percentile, and can be readily computed in Matlab using a built-in statistical software package. Similarly, the second intensity I_{high} is chosen such that 5% of all intensities are greater than I_{high} and is denoted the 95^{th} percentile. Note that the red/green ratio was used instead of the green channel alone, as it gave significantly better results.

For a given defined neighbourhood of the pixel region, all pixels that have a red/green intensity ratio lying in $[I_{low}, I_{high}]$ are selected. Out of this selection, all pixels that are "connected" to the current exudate region of interest are added. A pixel is "connected" to the given region if either the x distance or y distance to a pixel in that region is precisely equal to one pixel. The result of this method is given in Figure 5(b), which shows a significant amount of the exudates have been

captured. In particular, Figure 5(b) shows that larger exudates that are identified as several smaller regions are conglomerated into single identified exudate areas. Thus, where Figure 5(a) shows 4 potential exudates but identifies 8 separate regions, Figure 5(b) has aggregated them into 4 exudates.

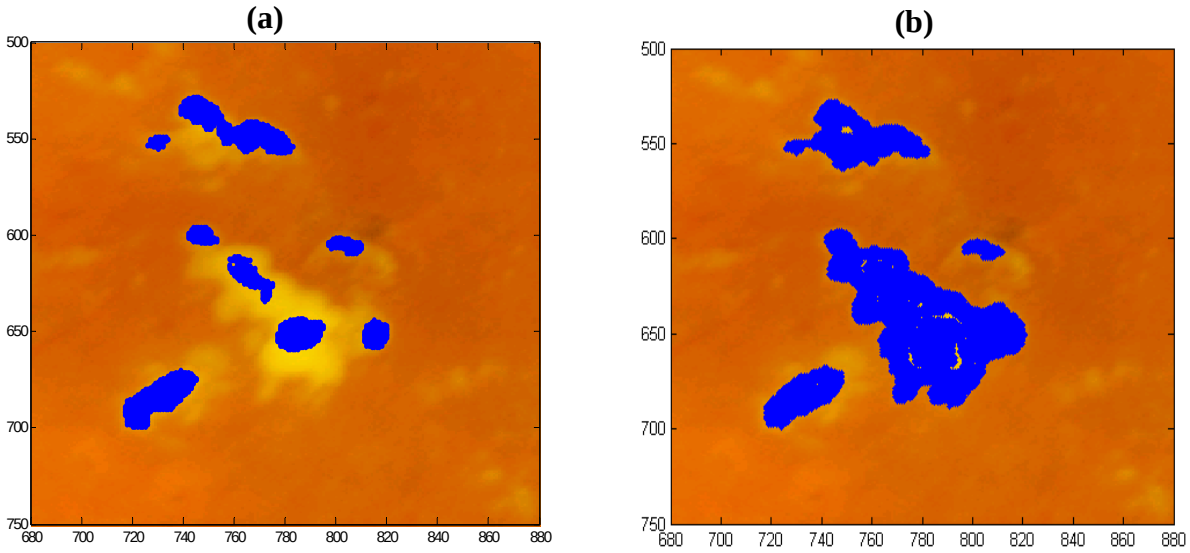

Figure 5: a) Example of applying median filter method of Figure 4; and b) the result after adding pixels

The final part of the algorithm uses a geometric image property of an exudate to rule out any remaining false exudates. The key property used to confirm the exudate is:

Property 1 – Consider a neighbourhood of the potential exudate. The contour of the red/green intensity surface, which has the largest mean absolute image gradient, is within a specified tolerance of the boundary of the exudate.

The neighbourhood of an exudate is defined to be the rectangle with a boundary 40 pixels from the unique rectangle precisely surrounding the identified exudate. Within the exudate neighbourhood, the contours of the red/green intensity surface are computed in steps of 0.05,

±0.5 around the mean red/green ratio of the exudate. Contours that are of sufficient length and are "nearby" the exudate are selected for further processing. These contours are considered "nearby" based on the distance from the centre of the unique circle, with radius $r_{exudate}$ precisely surrounding the exudate. Specifically, if any part of the contour is within a radius of $1.5*r_{exudate}$, the contour is selected as a candidate for the boundary of exudate. Once all the "nearby" contours are selected, the contour with the largest mean absolute image gradient is chosen. In addition, the contour must have a length of greater than 20 pixels.

Note that since the image gradient requires numerical differentiation, the image is first smoothed by a 6x6 median filter before taking the gradient. For example, Figure 6 (a) shows all selected candidate contours as dashed lines, the exudate is denoted by circles, and the blue solid line denotes the final chosen contour. In contrast, Figure 6(b) gives an example of the contours surrounding a false exudate. Notice that all the contours are very complex shapes and most are quite a distance away from the exudate. In this case, the solid blue contour corresponding to the largest mean absolute gradient is along a vein, yielding a long tubular shape that is also a considerable distance away from the exudate. Therefore, the false exudate can be ruled out using a distance metric between the contour and the exudate.

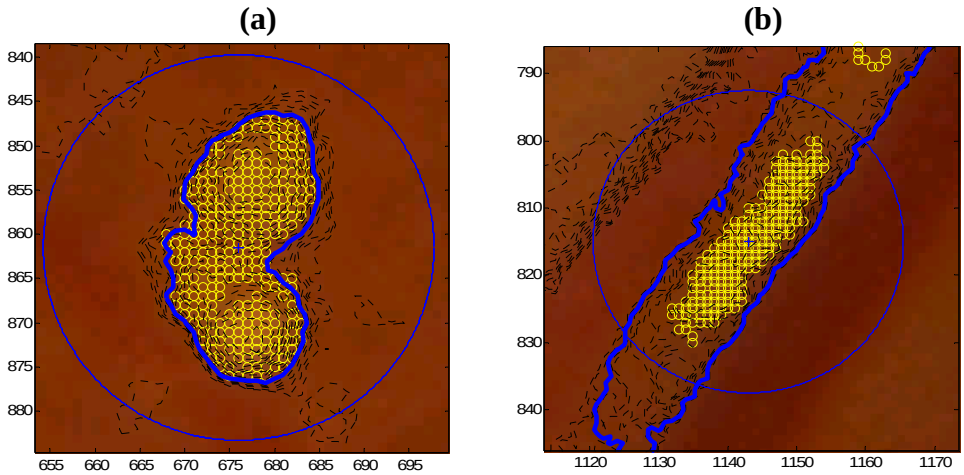

Figure 6: (a) Selecting contours of the red/green surface for a true exudate. Candidates contours are dashed lines, exudate is denoted by circles and blue solid line is the final chosen contour. (b) Contours of red/green surface for false exudate

The distance metric is defined based on the closest distance to an exudate point, for each point in the contour. Define:

$$C \equiv \{(x(i), y(i)), i = 1, \ldots, N\} \quad (1)$$

$$D_C = 75^{\text{th}} \text{ percentile of } \{d_{\text{exudate},i}, i = 1, \ldots, N\} \quad (2)$$

$$d_{\text{exudate},i} = \text{closest distance to exudate point from } (x(i), y(i)) \quad (3)$$

Any exudate that has a contour with $D_C > 4$ pixels in Equation (2) is removed, leaving only the true exudates.

For the case of Figures 6(a) and (b) the distances are $D_C = 1.00$ and $D_C = 13.03$ respectively. Hence, Figure 6(a) is kept as a true exudate and Figure 6(b) is removed.

2.2 Summary of Exudate Detection Algorithm

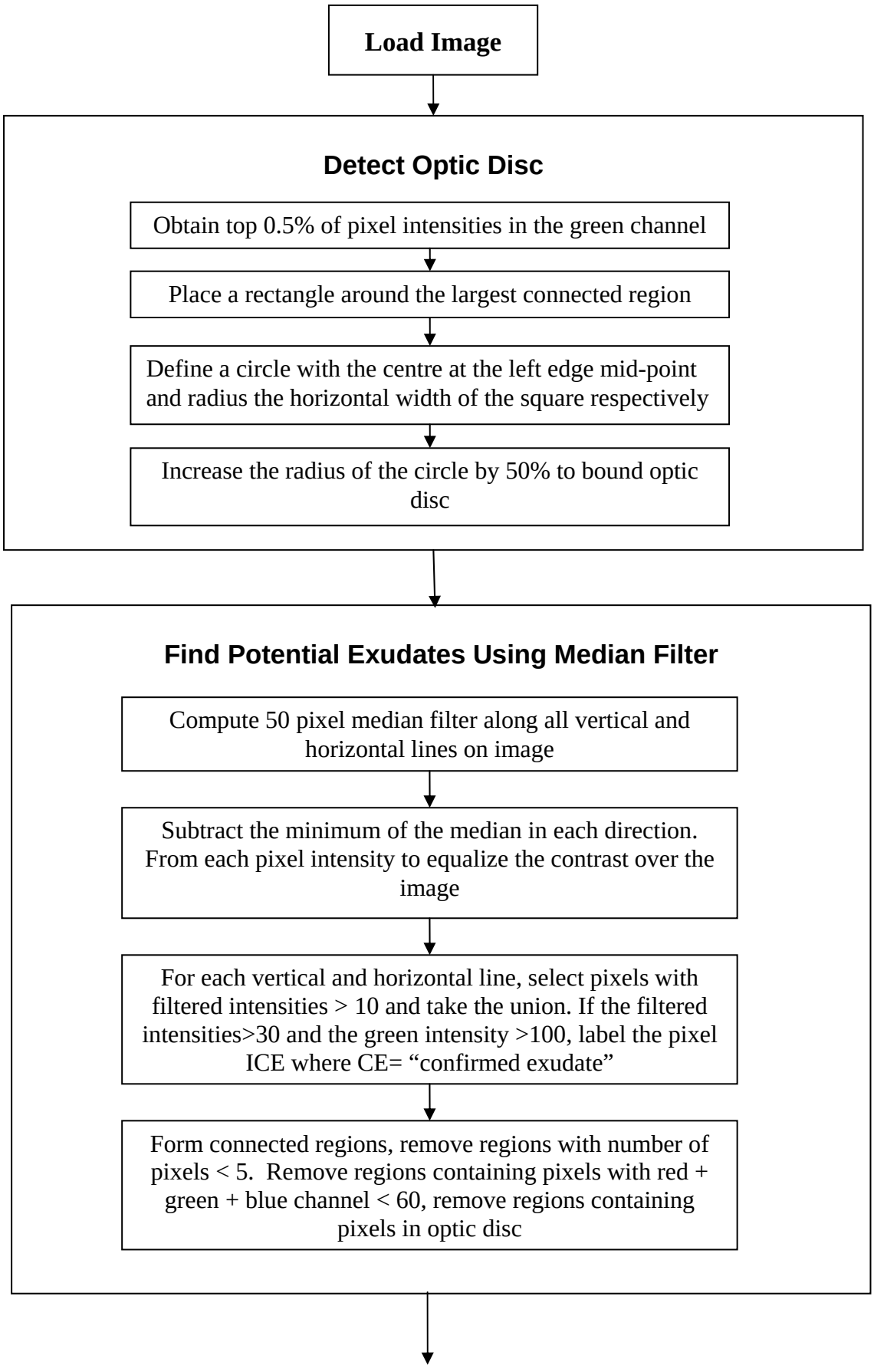

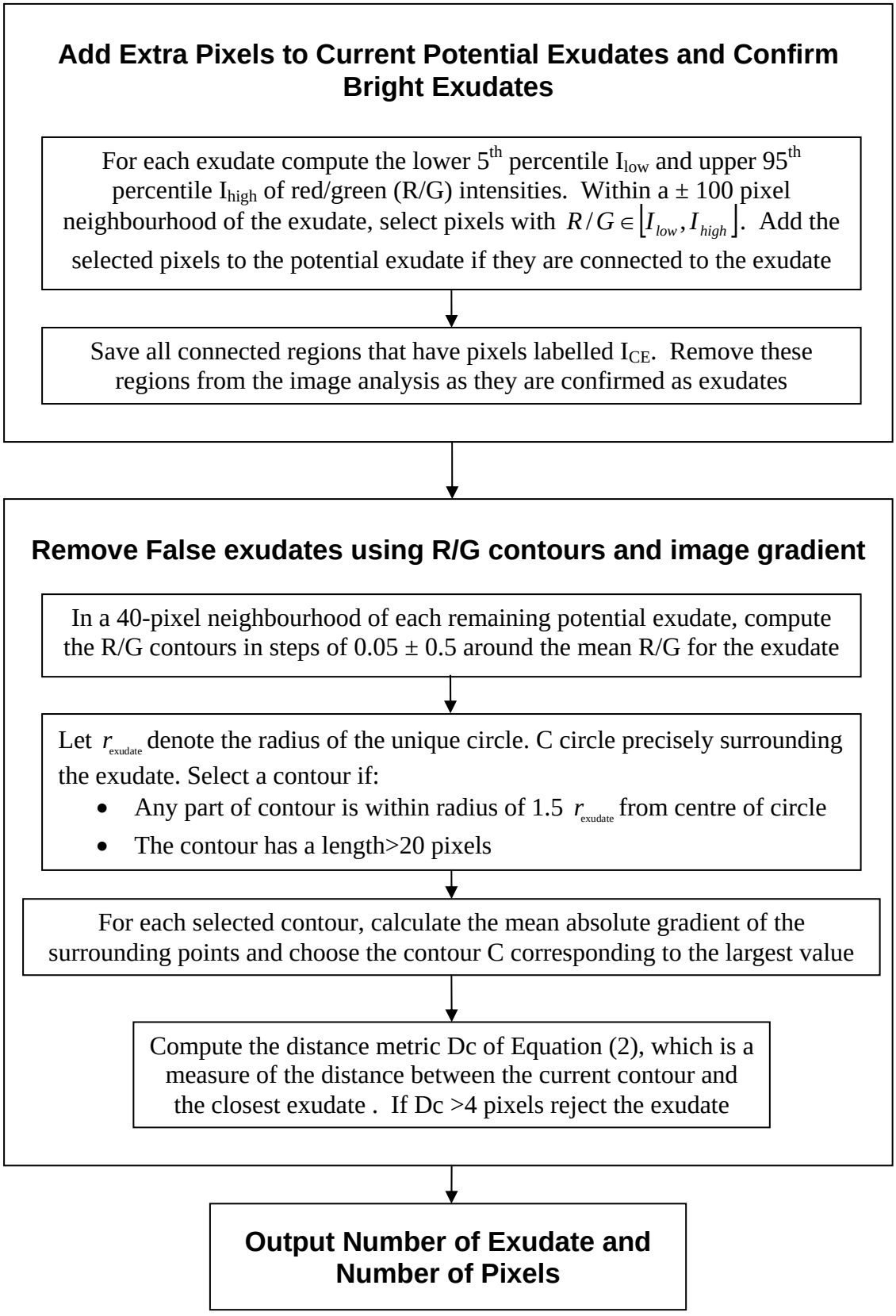

Figure 7: Algorithm for detecting exudates

2.3 Dot Hemorrhage Detection

Hemorrhages are a secondary sign of DR resulting from ruptured micro aneurysms, capillaries and venules. Classification of hemorrhages depends on their location within the retinal layers. DHs are located within the outer plexiform and inner nuclear layer. The loose arrangement of cells in these regions allows hemorrhages to assume the extracellular space. The roundish shape and distinct borders of DHs are due to intra-retinal compression confining the hemorrhage to a specific location.

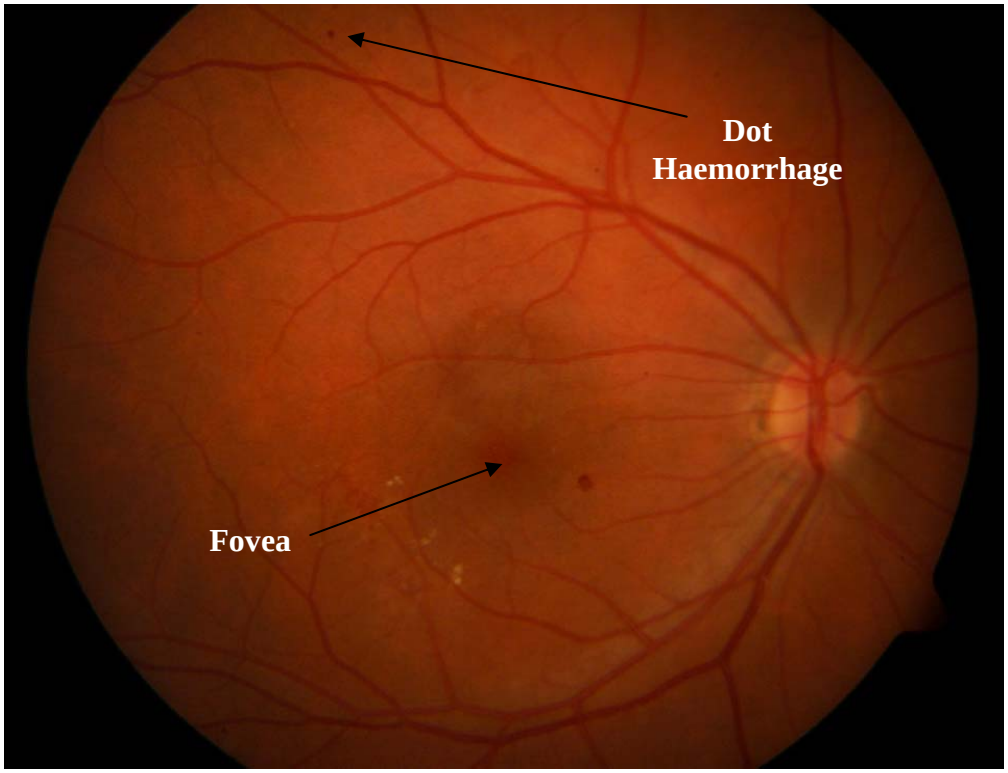

Figure 8: Fundus image with dot haemorrhages and fovea identified

As can be seen in Figure 8, DHs have a similar red colour to the vessels and are close to circular with reasonably well defined boundaries. This circularity is one of the physiological characteristics that can be readily used to segment the hemorrhages from other features in the image. The similarity in the colour between the DHs and the vessels makes it necessary to

accurately detect the vessels from the image before checking for DH. However, here again, physiological differences in shape can be an important and readily used classifier.

Segmentation is achieved in 5 main steps: 1) scaling and filtering, 2) thresholding, 3) shape selection, 4) vessel checking, and 5) contour checking. The ratio of the red to green intensities in the RGB image gives the best definition of the red features, and also has the added advantage of being more resistant to lighting changes between images. The spatial plot of the red/green ratio results in the brightening of the vasculature, hemorrhages, and the fovea pixels, which are predominantly red in colour, and dulls the optic disk and exudates, which are mostly yellow. An example image of the red/green ratio is given in Figure 9, which is the same image as in Figure 8, but processed. The significant brightening of the DHs and vessels significantly simplifies the choice of threshold to select the desired regions.

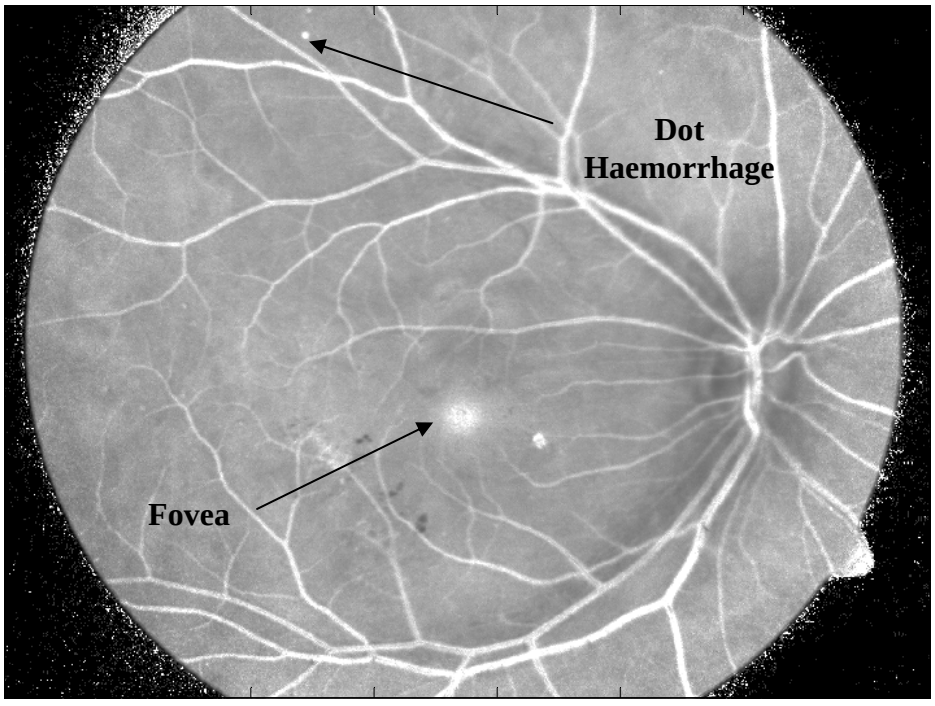

Figure 9**:** Image of the red green ratio intensities.

However, before choosing a threshold the image contrast is approximately equalized using a similar method to detecting exudates in the algorithm of Figure 7. Contrast equalisation is

achieved by first computing a 50 pixel median filter in the horizontal and vertical direction. The minimum of the median in each direction is then subtracted from the pixel intensity. This process is repeated for each pixel in the image. An example of the effect of this scaling on the intensities in the vertical direction is shown in Figure 10. The top 7% of the red to green intensities are then selected, which is shown in Figure 11. The value of 7% was based on experimental efforts with selected images, but quite accurately captures the majority of red features in all 100 fundus photographs in the database used here [20], including vessels and DHs. Therefore, at this stage there is no separation between the DHs and the vasculature.

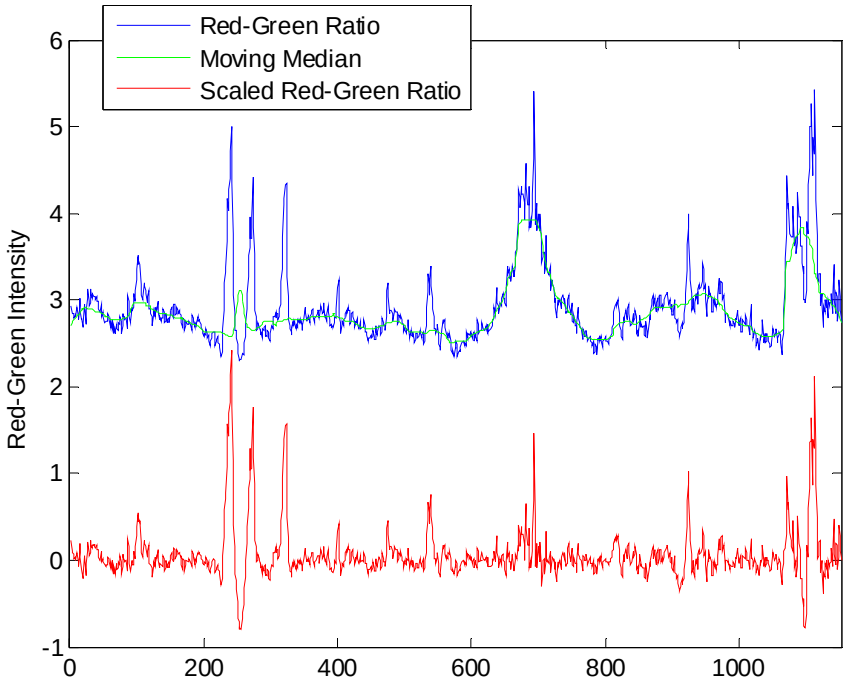

Figure 10**:** Scaling using a median filter on the red/green ratio in the vertical direction for one column of the image in Figure 9. No units are given as the y axis is a ratio which cancels out the units.

Note that the ratios in Figure 10 are much smaller than those in Figure 4, since in Figure 4 the values are the green intensities that can theoretically vary from 0 to 255. In most cases the red and green intensities are of a similar order of magnitude, so that their ratio is typically well less than ten and thus an order of magnitude smaller than the values in Figure 4.

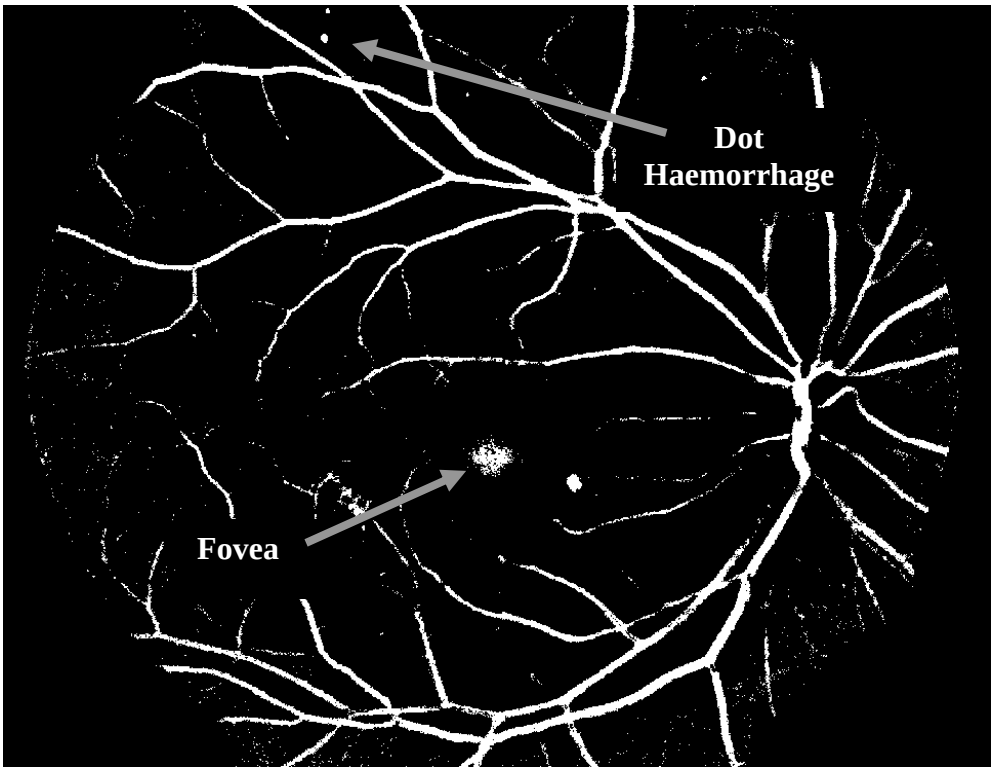

Figure 11**:** Binary image after thresholding

The next step is to label all the connected regions in Figure 11. The circular connected regions correspond to DHs. Therefore, any non-circular regions, such as blood vessels, are deleted from the image. The criteria for deleting a region is based on the shape factor, F_s defined:

$$F_s = \frac{A}{L_{\max}^{\ 2}} \tag{4}$$

where A is the area of the shape and L_{max} is the maximum distance between two pixels in a labelled region. Figure 12 shows three examples of the metric of Equation (4).

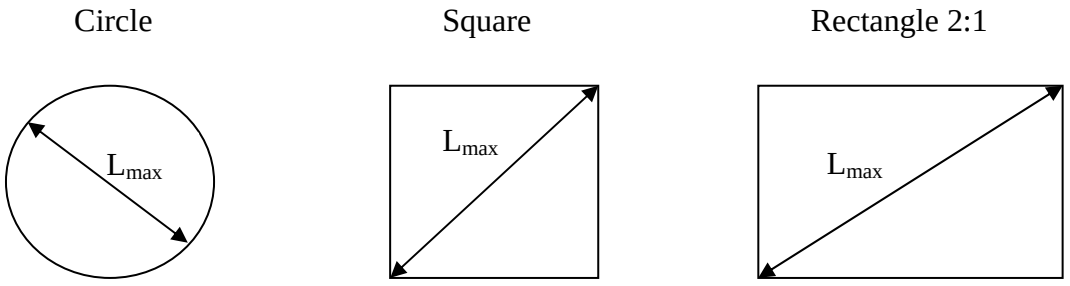

Note that the maximum value of F_s = 0.78 as expected, occurs for a circle. For simplicity in implementation , L_{max} is approximated as the maximum distance between pixels in the horizontal or vertical direction, and the area is the number of pixels, N_{pixel} that make up the shape. Therefore N_s in Equation (4) is redefined:

$$F_s = \frac{N_{pixel}}{\max[\{\max(x_{pixel}) - \min(x_{pixel})\}, \{\max(y_{pixel}) - \min(y_{pixel})\}]^2} \quad (5)$$

Equation (5) slightly changes F_s for the square and rectangle examples in [12]. The adjusted values are shown in Figure 13. The shape factor of a DH compared to a vessel and the fovea are shown in Figure 14. A shape factor threshold of 0.54 is used to segment the circular features from the unwanted red regions. The value of 0.54 was conservatively chosen to avoid false negatives.

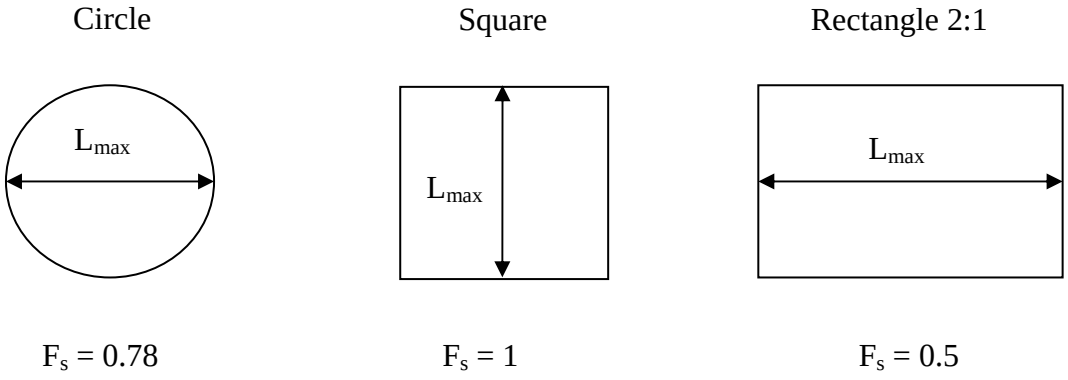

Figure 13: Simplified calculation of the shape number for a connected region

A given region in Figure 11 is deemed not to be a DH if the shape number of Equation (5) is less than 0.54. However, the remaining regions are still not necessarily a DH, as seen in Figure 15. The binary image of Figure 11 shows that the vasculature can be broken, or appear to be broken in the image, in places where it is clear a vessel should lie. In some cases the broken

vessel segment appears to be circular and is above the shape factor threshold. For example, the selected pixels in the region labelled “B” in Figure 15 are clearly a part of a blood vessel that is thus identified, where the region labelled “A” is clearly a DH. To rectify this problem a method of checking if the selected regions are on vessels is used.

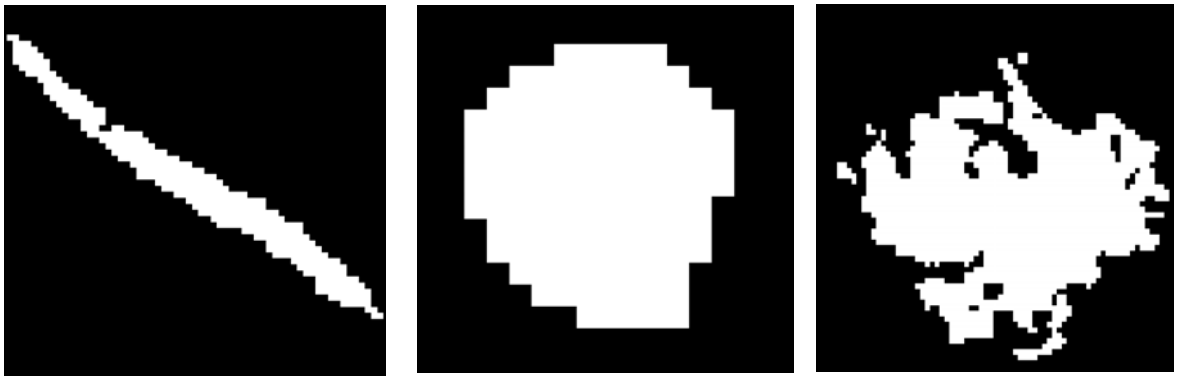

(a) F_s=0.097 (b) F_s=0.72 (c) F_s=0.44

Figure 14: Calculating the shape number for (a) a vessel, (b) a dot haemorrhage, (c) the fovea

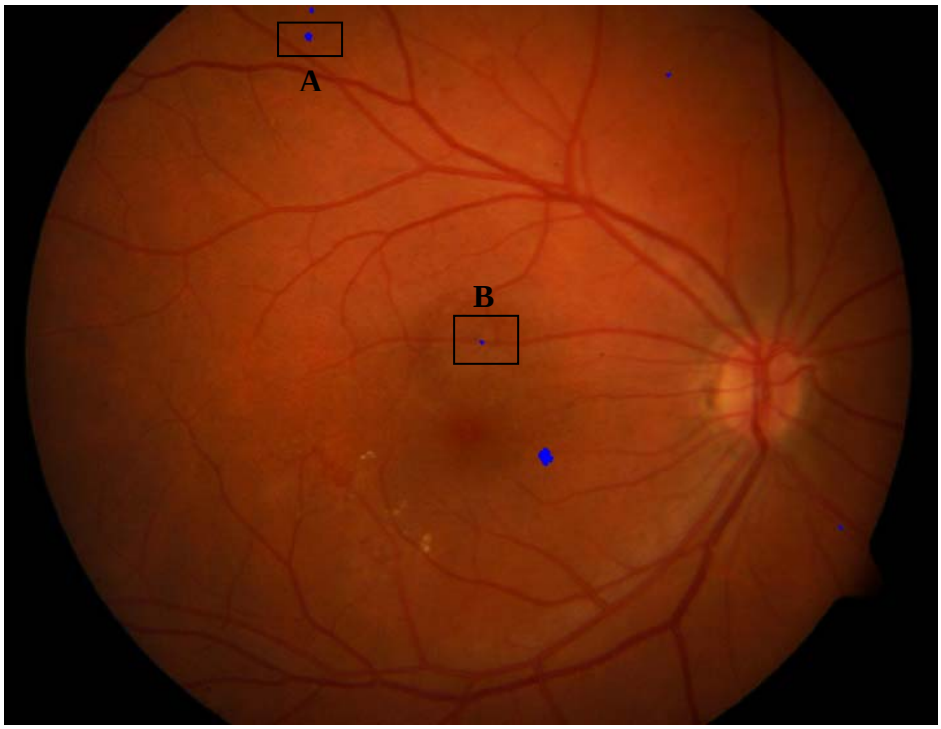

Figure 15 – Selection of the round regions

Vessel checking is done by finding the lines of minimum distance from the perimeter of a labelled region to the perimeter of its largest neighbouring region as seen in Figure 16. The

slope of the red to green ratio is then investigated along the line connecting the regions, as shown in Figure 17. If there is a sufficiently small difference in the red to green ratio along the line then the region is assumed to be part of a vessel and deleted from Figure 15. Figure 17 illustrates that there is little change in intensity of the red to green ratio along line 2 so the blue region in section B in Figure 15 can be said to be part of the blood vessel. However, there is a large dip in intensity along line 1 indicating that the blue region in section A is separate and not a part of a blood vessel.

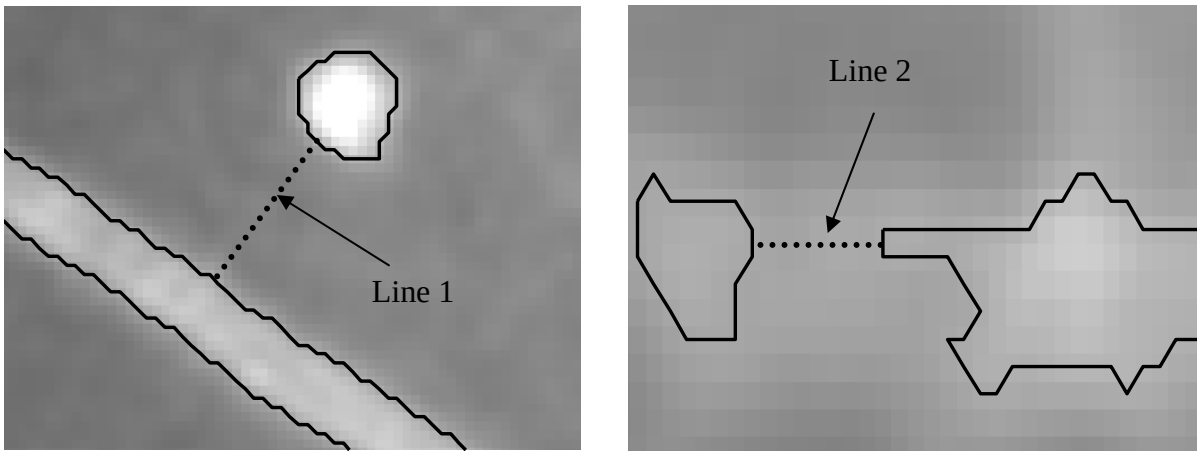

(a) section A from Figure 15 (b) section B from Figure 15

Figure 16: Results of minimum distance lines found from Delaunay triangulation

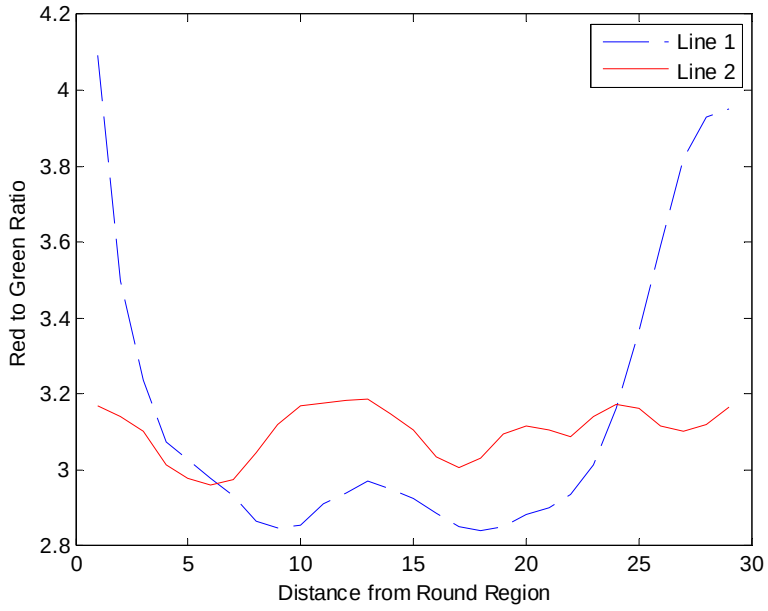

Figure 17: Red /green ratio intensity along lines 1 and 2

The same contour method shown in Figures 6 and 7 is then used to remove the regions that are not DHs. The final result is shown in Figure 18, which is the fully processed version of the original Figure 8. Figure 18 reveals the required DHs. Figure 19 summarises the overall DH detection algorithm. Note that this algorithm does not separate out microaneurysms, but their smaller size means a minimum size threshold could be used to potentially distinguish them from DHs. Future work will investigate the ability to accurately detect the smaller microaneurysms.

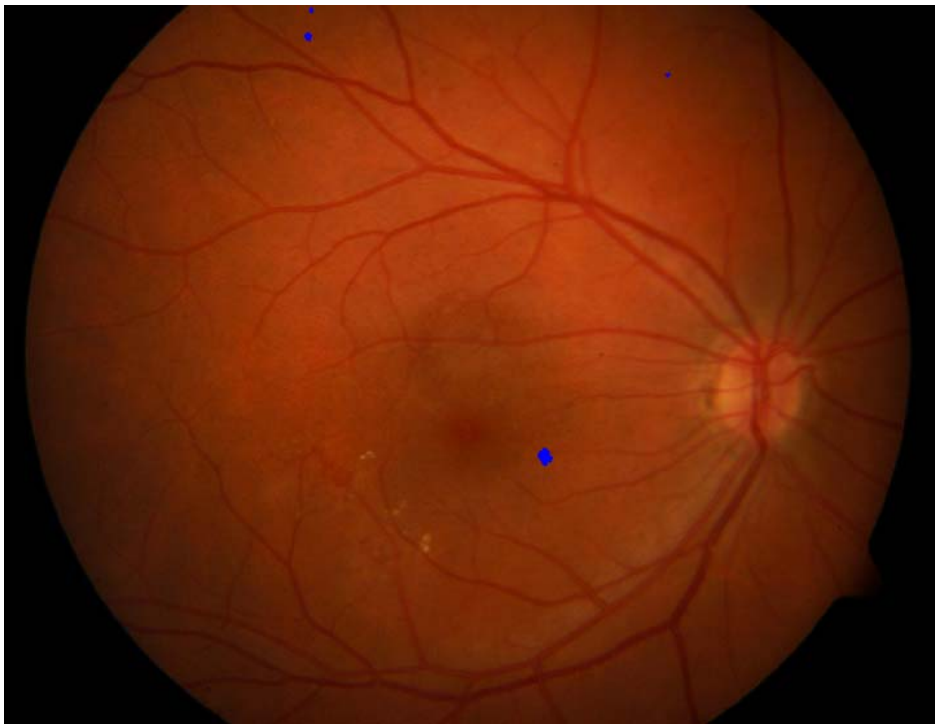

Figure 18**:** Dot haemorrhage segmentation from the fundus image

2.4 Summary of Dot Hemorrhage (DH) Detection Algorithm

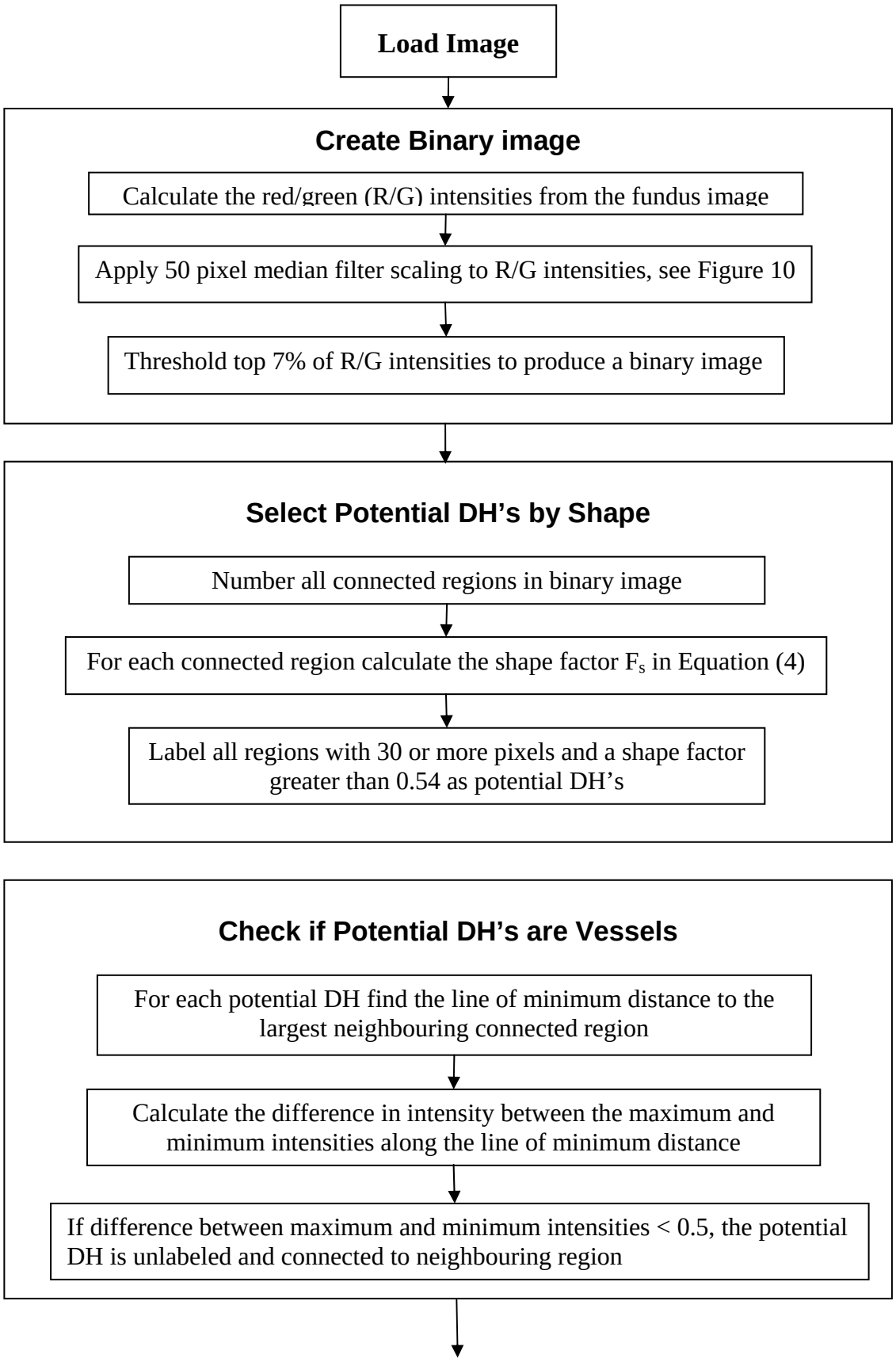

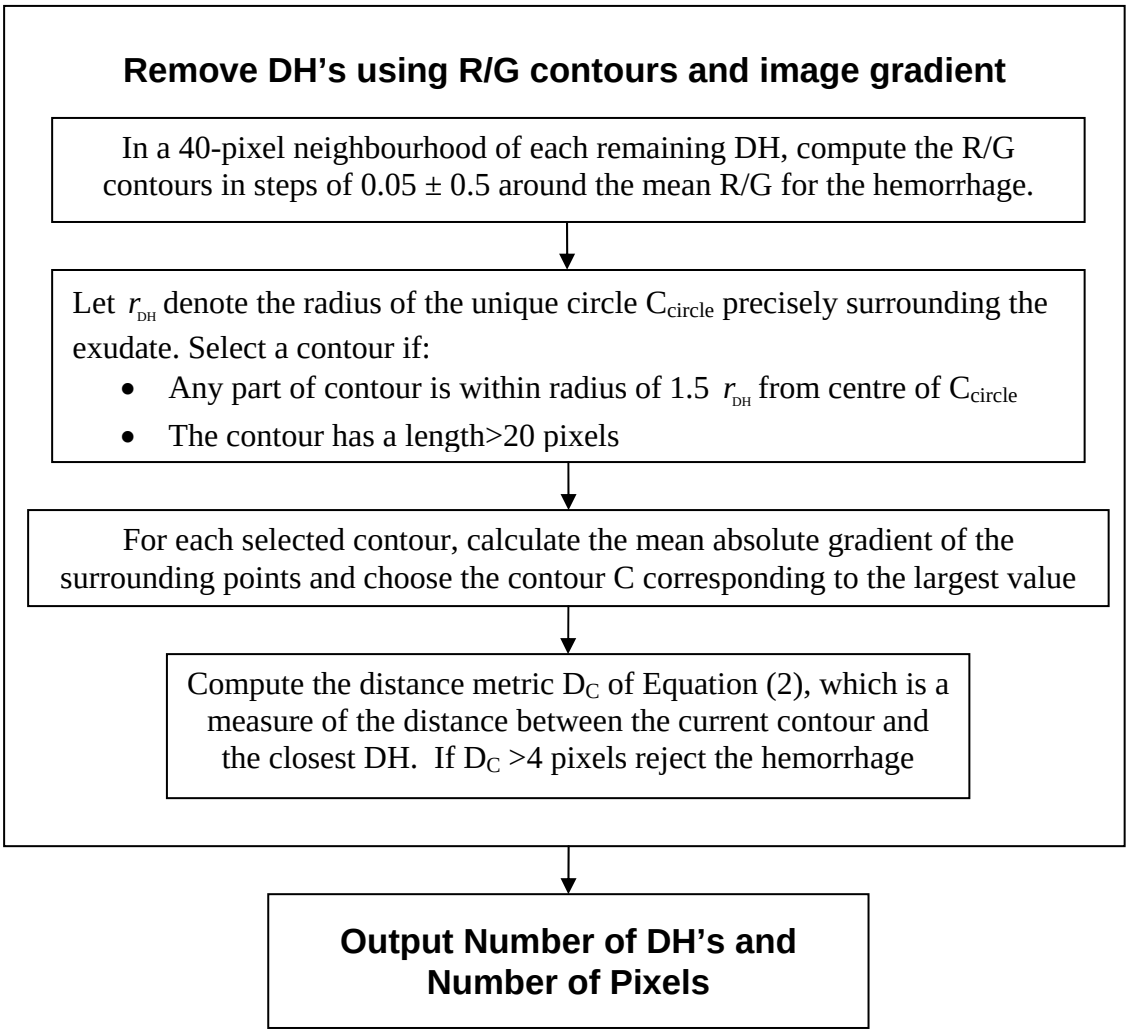

Figure 19: Summary of dot haemorrhage detection algorithm

2.5 Analysis and Validation

The methods are all implemented in Matlab (The Mathworks, Natick, MA, USA), a widely used numerical computing program. The algorithms of Figures 7 and 19 are tested on 100 images from the DiaretdbO_v_1_1 database [19, 20]. The results of the methods are evaluated using the ground truths, which were provided by clinical experts from this Finnish study [19].

Diagnostic results are measured in terms of: Specificity, Sensitivity, Positive Predictive Value (PPV) and Negative Predictive Value (NPV).

Clinically, diagnoses for these tests are based on existence, which only captures whether (or not) these phenomena are present, but not the number or size. The number and size might well have particular importance clinically over time, but are not currently utilised with any resolution in clinical practice. Thus, R1 and M1 diagnoses indicate the existence of one or more DHs (R1) or exudates (M1). The absence of DHs and exudates are diagnosed R0 and M0, respectively. Thus, if the images are considered as being sequential over time, they could also be used to diagnose the occurrence (or not) of new exudates and/or DHs, by highlighting changes in the patient's DR status from the prior imaging.

3.0 Results and Discussion

3.1 Exudate Results and Discussion

The algorithm of Figure 7 accurately detected the presence of exudates according to the diagnosis of [19, 20] with a sensitivity of 96.7% and a specificity of 94.9%. The results are summarized in Table 1.

Table 1: Sensitivity and Specificity of Algorithm

		Observed Diagnosis		
		M1	M0	
Algorithm	M1	59	2	PPV 0.97
	M0	2	37	NPV 0.95
		Sensitivity 96.7%	Specificity 94.9%	

Figure 20 (a) gives an example of an image that contains exudates that are hard to see and are in a dark part of the image, but the algorithm still accurately detects the presence of exudates. Figure 20 (b) shows that as well as detecting the presence of exudates, the actual number of exudates is closely captured.

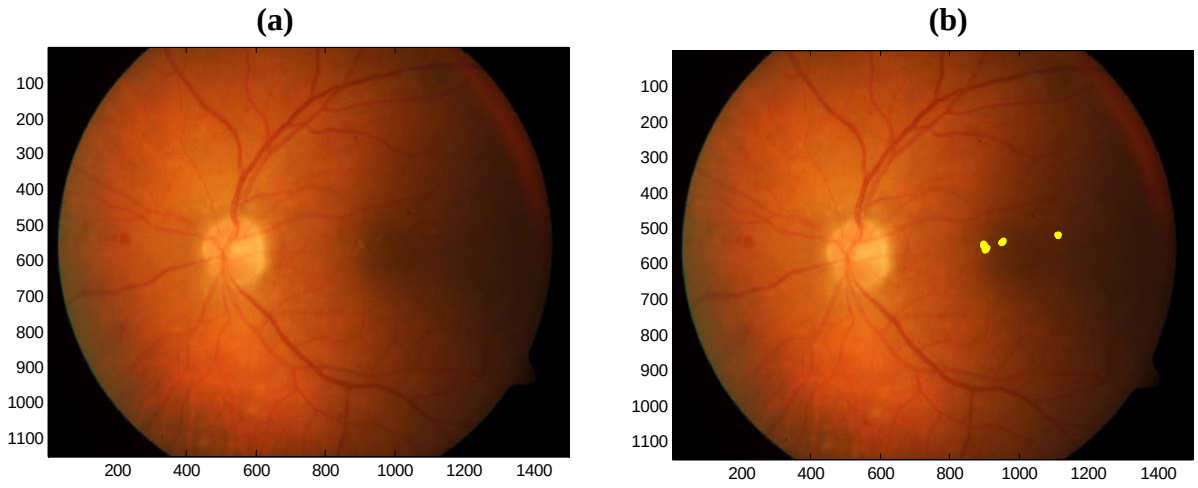

Figure 20: (a) Image 002, a darker image. (b) The results of the algorithm of Figure 7

The accuracy shown in Figure 20 (b) is typical over all images with the number of exudates found agreeing well visually. This result shows the potential for tracking the progress of DR. For example, the percentage of pixels covering exudates could be used as a metric for the degree of the disease but this application requires further clinical validation with specialists in the future.

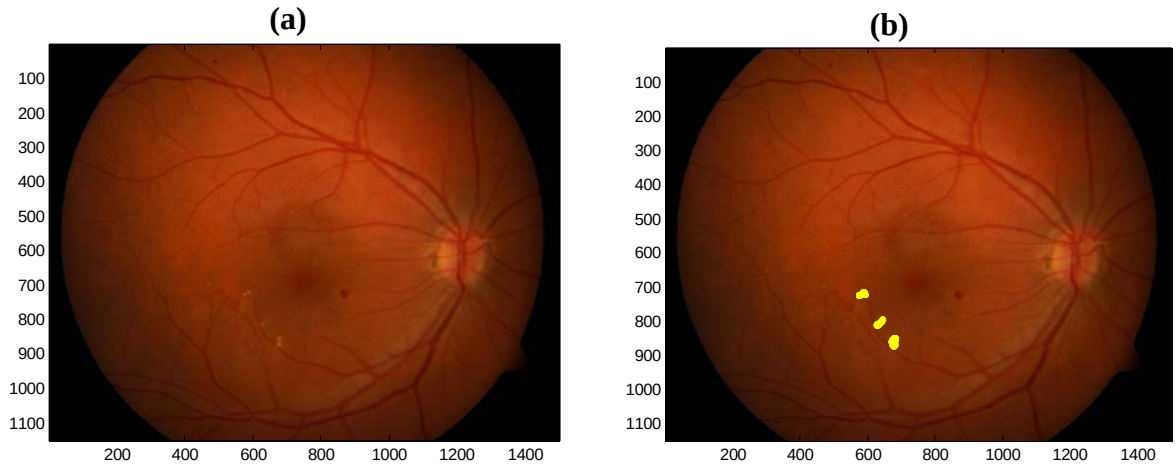

Figure 21: (a) image 005 (b) The results of the algorithm of Figure 7 on image 005 showing the actual number of exudates is accurately captured

One of the reasons for the significant accuracy of the method is the use of the contour finding routine as illustrated earlier in 6 (a) and (b). Figure 22 gives an example of the result of the algorithm of Figure 7 on Images 005 in Figure 21(a) without the contour checker, which shows that quite a number of false exudates are found. Notice that most of these false exudates lie along a vein. One potentially simple way of removing these is to check that it is within a specified tolerance of a vein. There are two problems with this. The first problem is that quite often an exudate can appear close to a vein, as is the case in Figure 21. The second problem is that any developed vein detector may miss the lighter veins. Hence, it is a non-trivial problem to remove these points without removing other true exudates. The end result is that for this image the algorithm would have counted more than double the number of exudates actually present. However, with the addition of the contour checker all the false exudates are easily removed, the final results given in Figure 21(b).

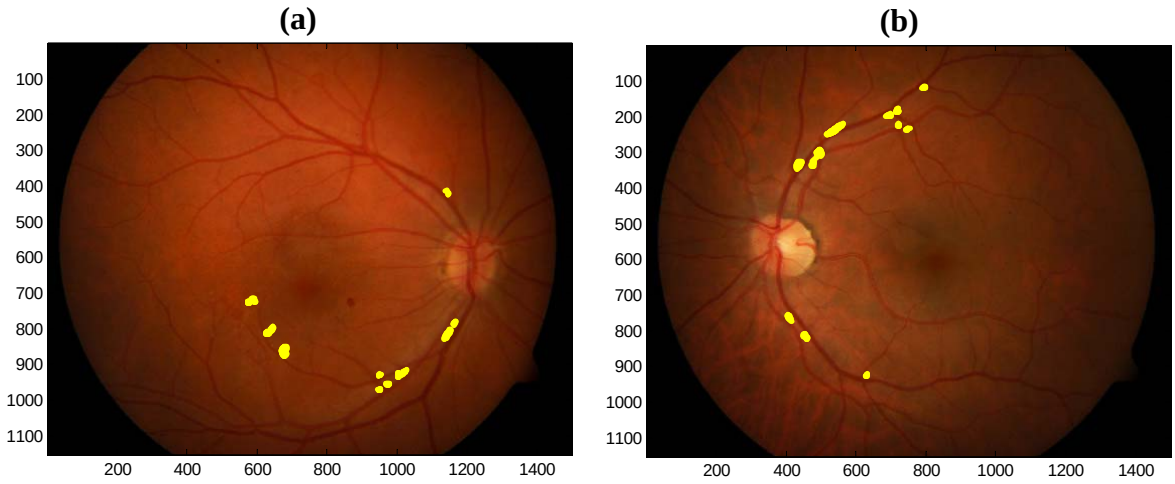

Figure 22 (a) An example of applying the algorithm of Figure 7 to Image 005 in Figure 21 without the contour checker. (b) Figure 7 applied to Image 099 without the contour checker.

Figure 22 (b) gives an example of the algorithm of Figure 7 without the contour checker applied to Image 099, which is clear of exudates. A number of false exudates are found, thus for this example a false positive would have occurred. With the addition of the contour checker all the false examples are removed (results not shown), leaving a clear image as required.

Note that there were two false positives and two false negatives found by the algorithm. Two examples of the images corresponding to a false positive and false negative are shown in Figures 23 (a) and (b). To the human eye, the yellow dot in Figure 23(a) looks like an exudate, and the fact that dot haemorrhages are also present confirms this possibility. However, the image was pronounced clear by the diagnosis in [19,20].

In contrast, it was claimed that image 71 contained exudates. However, as can be seen in Figure 24(b) it is very difficult to see exactly where these exudates are. Unfortunately, these images were not in the group of first 50 images that had marked exudates and dot haemorrhages. This latter result does show the potential efficacy or drawbacks of this approach, in that it is consistent without subjectivity. Thus, if image 71 has no exudates, as stated by the system, then it is showing the potential to avoid false positives, and vice versa.

Similar results occurred (not shown) for the other false positive and false negative. Hence, in the very small number of cases where the algorithm is wrong according to [19,20], the results are demonstrably arguable, demonstrating the inherent subjectivity involved in DR screening. Thus, no computer algorithm should be expected to fully agree with every ophthalmologist's observation in these types of cases, but do provide a consistent measure without subjectivity.

Figure 23 (a) A false positive (pointed to by an arrow) found by the algorithm of Figure 7 in Image 64. However, a potential exudate can be seen. (b) A false negative corresponding to Image 71. Dot haemorrhages can be seen, but it is hard to visually determine the existence of exudates.

3.2 Dot Hemorrhage Results and Discussion

For the first 100 from the DIARETDB0 database [19, 20], the algorithm of Figure 7 detected the presence of DHs accurately with no false positives and one false negative, as summarised in Table 2. The baseline for diagnosis was determined from [19, 20].

Table 2 – Processed Results of Algorithm for DHs

		Observed Diagnosis		
		R1	R0	
Algorithm Diagnosis	R1	1	24	PPV 96.0%
	R0	75	0	NPV 100%
		Sensitivity 98.7%	Specificity 100%	

The algorithm produced a sensitivity of 98.7% and a specificity of 100% when using DH to diagnose DR on a DH basis. The algorithm failed to correctly diagnose one image which contained a DH as seen in Figure 23. However, the DH is seen to lie in a dark region of the image shown by the labelled section “C”. As the DH lies in this dark region, the boundaries of the hemorrhage are not well defined. Therefore, when the fundus photograph is converted into a binary image the shape of the DH becomes distorted and the shape factor of Equation (2) rules the DH out. However, note that this DH is in fact likely a blot haemorrhage which is typically abnormally shaped.

Without the contour checker, the algorithm found 5 false positives. But in a similar way to the case of the exudates, the contour method as illustrated in Figures 6(a) and (b), easily removed these false points. On the other hand, the contour method presently only works on regions that have been identified. So it does not get rid of the false negative. However, simulations have shown that the contour method does not exclude these regions that were missed by the algorithm. Therefore, future work should include the contour method in the initial identification part of the algorithm.

Note that although there appears to be more than one DH in Figure 23, the other dark spots are not DH. These dark dots appear in most of the images in the database at the same location and are assumed to be associated with dust on the camera lens. Therefore, these spots are ignored when processing the results of the algorithm. In practice, the quality of the lens could be checked, for example, by taking a picture of a white page.

In summary, both methods of Figures 7 and 19 show good potential for detecting exudates and dot haemorrhages. The main weaknesses at this stage, include making no distinction between

drusen and exudates, and micro-aneurysms and dot haemorrhages. In addition, the focus was on developing the algorithms to recognise the presence or absence of DR. Although, most exudates and/or DH's agreed well to the first 50 marked images, and looked reasonable visually for the final 50 images, further validation is needed. In particular, the techniques presented may be required to be adapted to ensure accurate tracking of DR over time which is a completely different scenario. For example, previous history and knowledge of the patient's could be introduced into the algorithms to improve results. Other improvements to the algorithms would include utilizing more than one image per eye. However, the main advantages of the algorithms are that they are flexible and present a set of powerful analytical tools that could be adapted to different circumstances and be used to integrate more information on patients as it becomes available.

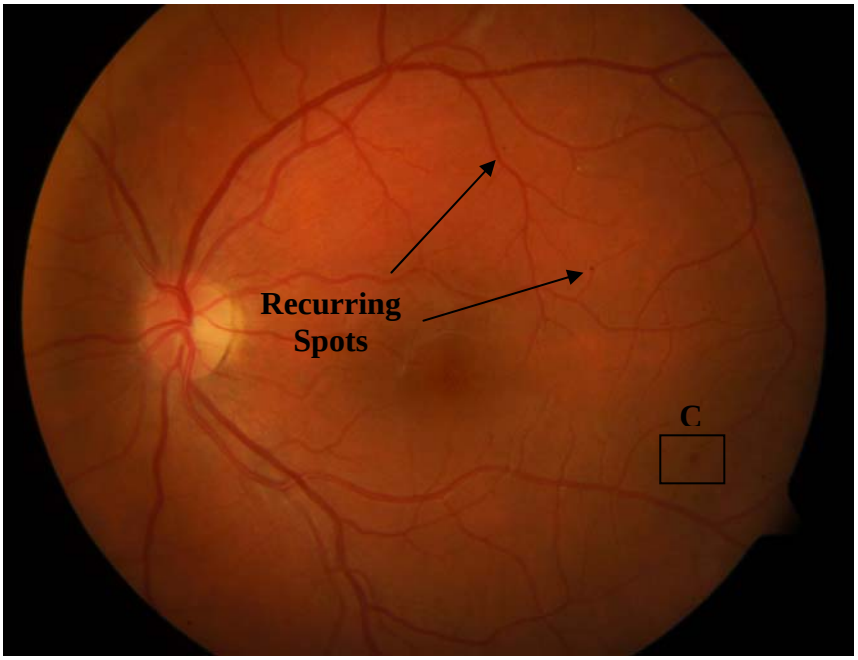

Figure 23: Fundus image of false positive

Finally, speed and computational time are important. Each image in the 100 image database was processed with this algorithm in approximately 40-80 seconds. Each image had 2 mega-

pixels of data, where current fundus images can be much larger if required. However, the algorithm was also not optimised for speed. Thus a 1 minute, on average, processing time occurs. With optimisation or the use of C a more powerful programming language instead of the user-friendly Matlab program, this time would be on the order of 1-10 seconds. Clinically, such turnaround times would enable the images to be taken and answer provided to the clinician, and expressed to the patient, in real-time while still in the office, if desired.

4.0 Conclusions

Automatic methods for screening exudates and DHs have been developed based on image processing methods that utilize colour, morphology and intensity gradients in fundus photographs. 100 images from a standard database were used to test the methods. For exudate detection, the clinical diagnostic sensitivity was 96.7% and specificity was 94.9%. For dot hemorrhage clinical diagnosis, the sensitivity was 98.7% and the specificity was 100%. From visual checks of the first 50 ground truth graded images, >95% of exudates/DHs were detected with virtually no false positives (<0.5%) which suggests the method could be used to accurately track changes over time. However, these results need to be validated in future clinical trials.

The reasons for the very high sensitivity with no false positives are the use of the red/ green ratio combined with a contour finding method and the image gradient after median filtering. The red/ green ratio has the advantage of helping to normalize out changes in light across the images and improves the contrast of DR features relative to the background. Additional filtering, using physiological and morphological details, reduced false positives without reducing true positive results. Furthermore, no statistical classifying methods were required.

The methods demonstrate a significant improvement over other algorithms in the literature and show potential for practical, clinical DR screening. The use of colour channels to directly identify DR lesions allows clinical expertise and observation to be directly incorporated into the algorithm, providing a potentially far superior result.

Finally, it is also obvious that further clinical testing and trials will be required to prove the algorithm in practice. However, the same approach can generalised to other manifestations of DR. The ability to detect the number and size of these manifestations implies further clinical outcomes will become available in terms of accurately tracking or monitoring the patient-specific evolution of DR.

References:

[1] Icks A, Trautner C, Haastert B, Breger M, and Gianni G (1997). "Blindness Due to Diabetes: Population based Age- and Sex- specific Incidence Rates," Diabetic Medicine, 14:571-575.

[2] Fong D, Aiello L, Gardner T, King G, Blankenship G, Cavallerano J, Ferris F, and Klein R (2004). "Retinopathy in Diabetes," Diabetes Care, 27:584-587.

[3] TEDPRG (The Eye Disease Prevalence Research Group), (2004). "The Prevalence of Diabetic Retinopathy Among adults in the United States," Archives of Ophthalmology, 122:552-563.

[4] Wild S, Roglic G, Green A, Sicree R and King H (2004). "Global Prevalence of Diabetes: Estimates for the year 2000 and projections for 2030," *Diabetes Care*, 27:1047-1053.

[5] Fong D, Aiello L, Gardner T, King G, Blankenship G, Cavallerano J, Ferris F, and Klein R (2003). "Diabetic Retinopathy," *Diabetes Care*, 26:226-229.

[6] Chia D and Yap E (2004). "Comparison of the Effectiveness of Detecting Diabetic Eye Disease: Diabetic Retinal Photography Versus Ophthalmic Consultation," *Singapore Medical Journal*, 45:276-279.

[7] ETDRSRG (Early Treatment Diabetic Retinopathy Study Research Group) (1991). "Early Photocoagulation for Diabetic Retinopathy," *Ophthalmology*, 98:766-785.

[8] Kertes PJ and Johnson TM (Eds.). "Evidence Based Eye Care," Lippincott Williams & Wilkins 2007.

[9] Hipwell J, Strachant F, Olson J, McHardy K, Sharp P, and Forrester J (2000). "Automated detection of microaneurysms in digital red free photographs: a diabetic retinopathy screening tool," *Diabetic Medicine*, 17:588-594.

[10] Abramoff MD, Niemeijer M, Suttorp-Schulten MSA, Viergever MA, Russell SR, and Van Ginneken B (2008). "Evaluation of a System for Automatic Detection of Diabetic Retinopathy From Color Fundus Photographs in a Large Population of Patients With Diabetes," *Diabetes Care*, 31(2):193-198.

[11] Kinyoun JL, Martin DC, Fujimoto WY, and Leonetti DL (1992). "Ophthalmoscopy Versus Fundus Photographs for Detecting and Grading Diabetic Retinopathy," *Investigative Ophtalmology & Visual Science*, 33(6): 1888-1893.

[12] Moss SE, Klein R, Kessler SD, and Richie KA (1985). "Comparison between ophthalmoscopy and fundus photography in determining severity of diabetic retinopathy," *Ophthalmology*, 92:62-67.

[13] Sanchez C, Hornero R, Lopez M, Aboy M, Poza J, and Abasolo P (2007). "A Novel Automatic Image Processing Algorithm for Detection of Hard Exudates based on Retinal Image Analysis" *Medical Engineering and Physics*, Vol. 30:350-357.

[14] Walter T, Massin P, Erginay A, Ordonez R, Jeulin,C, and Klein J (2007). “Automatic Detection of Microaneurysms in Colour Fundus Images,” *Medical Image Analysis*, 11:555-566.

[15] Sinthnayothin C, Boyce J, Williamson T, Cook H, Mensah E Lal S, and Usher D (2002). “Automated Detection of Diabetic Retinopathy on Digital Fundus Images,” Diabetic Medicine, 19:105-112.

[16] Frame AJ, Undill PE, Cree MJ, Olson JA, McHardy KC, Sharp PF, and Forrester JF (1998). “A comparison of computer based classification methods applied to the detection of microaneurysms in opthalmic fluorescein angiograms,” *Computers in Biomedical Research*, 28:225–238.

[17] Gardner GG, Keating D, Williamson TH and Elliott AT (1996). “Automatic detection of diabetic retinopathy using an artificial neural network: a screening tool,” *Br J Ophthalmol*, 80(11):940-944.

[18] Ege BM, Hejlesen OK, Larsen OV, Moller K, Jennings B, Kerr D, and Cavan DA (2000). ”Screening for diabetic retinopathy using computer based image analysis and statistical classification,” *Computer methods and programs in Biomedicine*, 62; pp. 165-175.

[19] Kauppi T, Kalesnykiene V, Kamarainen JK, Lensu L, Sorri I, Uusitalo H, Kalviainen H, and Pietila J (2006). “Evaluation Database and Methodology for Diabetic Retinopathy algorithms,” Technical Report, URL: http://www.it.lut.fi/ project/imageret/diaretdb0/.

[20] Kauppi T, Kalesnykiene V, Kamarainen JK, Lensu L, Sorri I, Raininen A, Voutilainen R, Uusitalo H, Kalviainen H, and Pietila J (2007). “The DIARETDB1 diabetic retinopathy database and evaluation protocol,” *Proc. of the British Machine Vision Conf (BMVC2007)*, Vol. 1, pp. 252-261.

[21] Niemeijer, M. Ginneken, BV, Russell, SR, Suttorp-Schulten, MSA and Abramoff, MD (2007). “Automated Detection and Differentiation of Drusen, Exudates, and Cotton-Wool Spots in Digital Color Fundus Photographs for Diabetic Retinopathy Diagnosis,” *Invest Ophtalmol Vis Sci.*, Vol 48, pp. 2260-2267.